Available online at www.sciencedirect.com
SCIENCE DIRECT®
International Journal of Heat and Mass Transfer 47 (2004) 5085–5093
International Journal of HEAT and MASS TRANSFER
www.elsevier.com/locate/ijhmt

A new methodology for experimental determination of liquid–gas interphase positions on a heated solid

M.E. Rojas [a,*], M.C. de Andrés [b]

[a] Department of Renewable Energy, CIEMAT, Avda. Complutense 22, 28040 Madrid, Spain
[b] Grupo de Energías Renovables, Facultad de Físicas. U. Complutense, 28040 Madrid, Spain

Received 24 February 2004; received in revised form 4 June 2004
Available online 13 August 2004

Abstract

In this paper a new methodology is presented to experimentally quantify liquid front positions on a heated solid when working under two-phase flow conditions. Applicable to solids, of which one dimension can be considered infinite (2D-solids), this methodology uses a unidimensional temperature profile measured inside the solid, which is interpreted with the aid of a newly defined parameter, cof^*h. The parameter cof^*h is an effective heat transfer coefficient in the framework of a unidimensional heat balance model. The values and profile of the parameter cof^*h reflect the different effectiveness in heat transfer of a heated surface when in contact with a liquid phase (wet surface) and when in contact with a gas phase (dry surface), thus making it possible to determine the position of the liquid front for every surface of such a 2D-solid. The accuracy of this method depends, mainly, on the conductivity of the solid and, secondly, on the distance between temperature gauges. The methodology has been validated with a commercial finite element analysis code and has been applied to locate experimentally the portion of the inner and outer wet surfaces of two horizontal pipe samples immersed in water under different operational temperatures. One of the samples is a normal smooth carbon steel pipe, while the other has microchannels grooved in its inner surface. The microchannels help to develop capillary forces that keep the inner surface wet above the horizontal water level at which the sample is immersed. The difference in liquid limit between the inner and outer surfaces can easily be determined by the parameter cof^*h. The method proposed is especially usefull when visual methods cannot be used.

1. Introduction

There are several areas of scientific investigation in which it is important to know which portion of a heated surface is wet. Basically these areas concern two-phase flows and flows induced by capillary forces. The importance of such knowledge lies in the fact that coefficients of heat transfer between a solid and a liquid phase are much greater than between a solid and a gas phase. In horizontal pipes working under two-phase flow, the flow pattern—annular or stratified—is critical for the effectiveness of the transference of an external flux to the fluid inside the pipe. The investigation of the effectiveness of capillary forces for inducing flows over surfaces has intensified in the last two decades with regard to possible applications in heat pipes used in modern air

* Corresponding author. Tel.: +34 91 3466049; fax: +34 91 3466037.
E-mail addresses: esther.rojas@ciemat.es (M.E. Rojas), mcandres@fis.ucm.es (M.C. de Andrés).

0017-9310/$ - see front matter © 2004 Elsevier Ltd. All rights reserved.
doi:10.1016/j.ijheatmasstransfer.2004.06.011

Nomenclature

Δs^*	effective element surface (m^2)
ΔV	element volume (m^3)
cof^*h	effective heat transfer coefficient ($W/m^2\,K$)
G	net power per unit volume (W/m^3)
G_0	external power supply per unit volume (W/m^3)
k	thermal conductivity of the solid ($W/m\,K$)
Q^{lost}	power lost per unit volume (W/m^3)
r	radial coordinate
z	coordinate along which the solid is considered infinite
T	temperature (°C, K)
x, ζ	coordinates along which the solid–liquid–gas interphase is situated

Superscript

*	related to a measured/simulated magnitude

Subscripts

A	related to zone A
B	related to zone B
C	related to zone C
j	related to an element
max	maximum
sat	related to saturation or operating conditions

conditioning systems and thermal solar collectors. Capillary forces can be promoted by porous coatings and by microchannels.

In the case of two-phase flows, most experimental devices for determining how wet a heated surface is, are flow visualisations with non-intrusive optical methods. These methods make use of an optical fibre [1], or a video camera, with which the two-phase flow developping inside a transparent tube is recorded [2–4]. At the HIPRESS facility [5], flow visualisations are obtained by a Radiometric Densitometer (RaDiMe), which compares the X-ray attenuation by every involved phase. In flows induced by capillary forces, visual observations at atmospheric pressure are the easiest method for measuring capillary rise [6,7]. Some researchers [1,8]—whose aim is to determine heat transfer coefficients for the different phases—measure a temperature profile and use a bidimensional heat balance model. The dissimilarity in heat transfer coefficients thus obtained shows how wet the studied surface is.

This paper describes a new methodology for determining how wet the surfaces of a heated solid are. Like the aforementioned, this methodology involves measuring a unidimensional temperature profile, but this is done in the framework of a unidimensional heat balance model. It has the advantages of reducing the complexity of the heat balance model involved and of permitting greater flexibility in positioning the temperature gauges in the 2D-solid. This methodology is based on the interpretation of a newly defined parameter cof^*h which represents an effective heat transfer coefficient.

2. Conceptual definition of the parameter cof^*h

Let us consider a solid which is infinite in one of its dimensions (which in Fig. 1 would be the z-coordinate), and of which one surface is in contact with a liquid upto a position x_A, and the other one upto a position x_B. Three different zones of the solid can be distinguished: zone A ($0 \leqslant x \leqslant x_A$), where both surfaces are wet; zone B ($x_A \leqslant x \leqslant x_B$), where one surface is wet and the other is dry or in contact with the gas phase; and zone C ($x_B \leqslant x \leqslant x_{max}$), where both surfaces are in contact with the gas phase. Let us also assume that the solid is heated by a constant and uniform external heat flux or

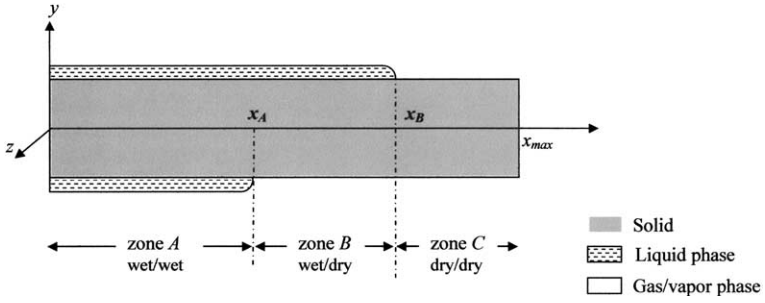

Fig. 1. 2D-solid diagram with its two surfaces wet up to different positions.

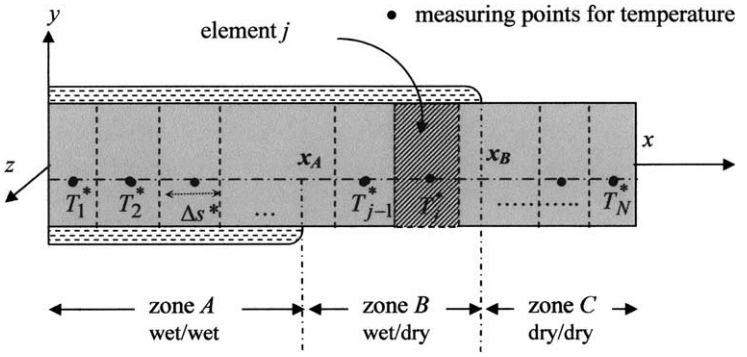

Fig. 2. Nodes/gauges positioning to have an unidimensional temperature profile.

that it is a constant and uniform heat generating source itself. Such energy has to be transferred to its surroundings, i.e., to the liquid or to the gas phases, which are considered to be at a certain saturation temperature, T_{sat}.

With the proposed methodology, one can determine the liquid front positions on both surfaces, x_A and x_B, when visual observations are not possible. It is based on the interpretation of an experimental unidimensional temperature profile, $\{T_j^*\}$, which can be obtained by inserting temperature gauges (thermocouples or Pt-100) into the solid up to a certain fixed inner position (Fig. 2).

Let us consider the solid divided in elements along the x-coordinate (Fig. 2). At every experimental temperature node, T_j^*, Laplace's equation gives the heat balance for every element j by

$$k\nabla^2 T_j^* + G_j = 0 \tag{1}$$

where k is the conductivity of the solid and G_j accounts for the sources and drains of energy per unit of volume in every element. The energy drains are nothing other than the heat transferred to the surroundings of the solid, Q_j^{lost}. This loss of energy can be defined by an effective heat transfer coefficient, cof^*h—effective because it takes the losses of both surfaces of the solid into account and relates them to the measured temperature T_j^*—and be expressed as follows:

$$Q_j^{lost} = cof^*h\Big]_j \cdot \left(T_j^* - T_{sat}\right)\frac{\Delta s^*}{\Delta V} \tag{2}$$

where Δs^* is the effective element surface at measuring point (Fig. 2), and ΔV is the volume of the solid element. The effective heat transfer coefficient, cof^*h, depends on the superheating of the solid on both of its surfaces (i.e., on the difference between its temperatures on its surfaces and the saturation temperature at which the fluid is considered to be) and on the real convection heat transfer coefficients between the solid and the fluid surrounded it (liquid or gas). The net energy of the system can be described by the following equation, in which G_0 is the constant and uniform energy generated or applied to the solid per unit of volume:

$$G_j = G_0 - cof^*h\Big]_j \cdot \left(T_j^* - T_{sat}\right)\frac{\Delta s^*}{\Delta V} \tag{3}$$

Eq. (1) becomes, therefore,

$$k\nabla^2 T_j^* + G_0 - cof^*h\Big]_j \cdot \left(T_j^* - T_{sat}\right)\frac{\Delta s^*}{\Delta V} = 0 \tag{4}$$

Extracting the term $cof^*h]_j$ we can establish that

$$cof^*h]_j = \left[k\nabla^2 T_j^* + G_0\right]\frac{\Delta V/\Delta s^*}{\left(T_j^* - T_{sat}\right)} = 0 \tag{5}$$

This expression enables us to calculate the effective heat transfer coefficient, cof^*h, for every element from an experimental temperature profile inside the solid, $\{T_j^*\}$. For the same fluid, heat transfer coefficients between solid and liquid phase are, at least, one order of magnitude higher than heat transfer coefficients between solid and gas phase. Such different orders of magnitude should be reflected in the values of the parameter cof^*h, as it represents an effective heat transfer coefficient. Therefore, the values of cof^*h for the elements situated in the zone A (wet/wet) should be higher than the values for the elements in zone B (wet/dry). The values of cof^*h for the elements in zone C (dry/dry) should be the lowest ones because, in this zone, both surfaces of the solid are in contact with the gas phase. In other words, the profile and values of the parameter cof^*h along the coordinate where the liquid–gas interphase is situated (x-coordinate in Figs. 1 and 2) are expected to give the necessary information to locate both liquid fronts in the above general case, positions x_A and x_B.

3. Validation with simulated results (obtained by ANSYS® code)

ANSYS® is a commercial finite element model programme developed by Swanson Analysis Systems, Inc.

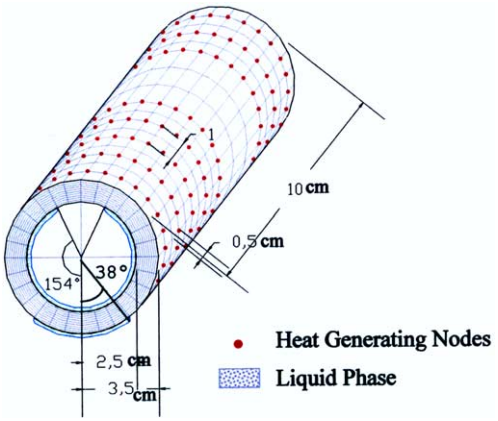

Fig. 3. Finite element model figure for simulating a heated carbon and steel pipe.

(SASI). With this software, a sample pipe of carbon steel, with an inner/outer diameter of 50/70 mm and a length of 10 cm has been simulated. An external total heat power of 536 W is applied by 280 external generating nodes, grouped in 10 rings with 1 cm between them. The fluid considered is water (liquid and vapor). The inner tube surface is assumed to be wet up to 154.3° from the bottom and the outer surface up to 38.6° (Fig. 3). Both the liquid and gas phases are assumed to be at saturated conditions at 311 °C (T_{sat}).

The heat transfer coefficients used between the solid and the gas phase are based on the Fishenden & Saunders' expression for laminar natural convection [9]. The heat transfer coefficients when the solid is wet are based on the expression by Rohsenow [10], for nucleate boiling conditions and the one given by Bromley [11], for liquid film boiling conditions—once the critical heat flux is reached.

With cylindrical coordinates, (r, ζ, z), we obtained simulated temperature data every $\Delta r = 10^{-3}$ m, $\Delta\zeta \approx 12.8°$ and $\Delta z = 5 \times 10^{-3}$ m. Along the sample (z-coordinate) a teeth external temperature map appears (Fig. 4(a)), with the crests coinciding with the rings where the energy generating nodes are. To justify the assumption of a 2D-solid, i.e. a solid which is infinite in one of its coordinates, we work with the temperature profiles at $z = 5 \times 10^{-2}$ m (at half the length of the sample), which are not affected by border length effects (Fig. 4(b)). As expected, the temperature profile is symmetric with respect to the vertical, and therefore only the variation in the angle, ζ, between 0° and 180° (15 nodes) has to be taken into account. At this z-position, to have a unidimensional temperature profile, one can consider any of the radial temperature profiles within the solid, i.e., $\{T(r = r^*, \zeta_j)\} = \{T^*(\zeta_j)\} = \{T_j^*\}$ with the possibilities of 25×10^{-3} m $< r^* < 35 \times 10^{-3}$ m. Under these considerations, we can verify the ability of the parameter cof^*h to determine the liquid front positions on the inner ($\zeta_B = 154.3°$) and outer ($\zeta_A = 38.6°$) surfaces of the solid.

The term $\nabla^2 T_j^*$ in Eq. (5) can be calculated by different methods. The values cof^*h shown in Fig. 5 have been calculated using a Taylor's series to obtained the term $\nabla^2 T_j^*$ where it was taken into account that this term for a fixed radial position, r^*, depends only on angular positions, ζ. In the cof^*h profies obtained for every r^* the three zones—zone A (wet/wet), zone B (wet/dry) and zone C (dry/dry)—can be distinguished by two slope sign changes. For lower angles (zone A) the cof^*h curve is nearly horizontal, with a slight positive slope and with numerical values typical of heat transfer coefficients between solid and liquid ($\sim 10^3$ W/m^2 K). Just before reach-

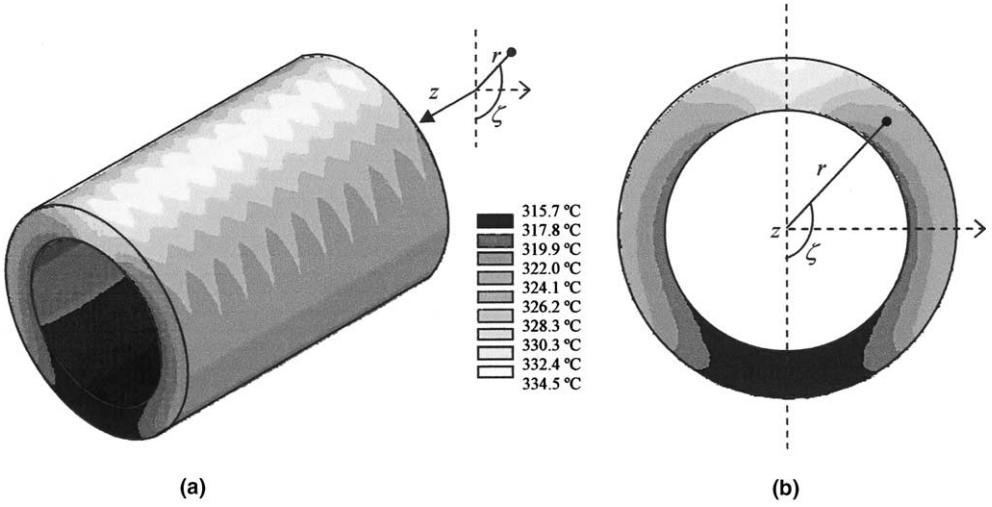

Fig. 4. Simulated thermal maps obtained by ANSYS. (a) Whole sample, (b) cross-section at $z = 5 \times 10^{-2}$ m.

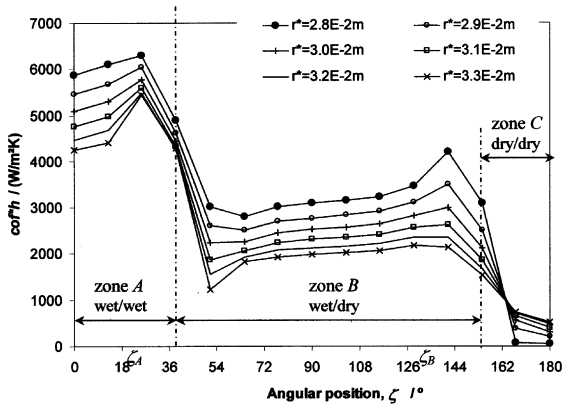

Fig. 5. Parameter cof^*h versus angular position. Values obtained using Eq. (5) and simulated temperature profiles at $z = 5 \times 10^{-2}$ m.

ing the external wet front ($\zeta_A = 38.6°$) the slope of the cof^*h profile changes its sign and the numerical values drop. From here onwards only the inner surface is wet while the outer is dry (zone B). At the border between the wet and dry zone of the inner surface (i.e. around $\zeta_B = 154.3°$) the second drop in cof^*h values appears. In zone C, cof^*h has typical values for solid to gas phase heat transfer coefficients (<1000 W/m^{2}K). These two slope sign changes are situated at the same angular positions for every thermal profile, independently of the radial position (r^*) chosen.

Therefore, if we were not dealing with simulated data but with experimental data, i.e., if we did not know a priori the exact values for both liquid fronts ($\zeta_A = 38.6°$ and $\zeta_B = 154.3°$) and we had a temperature profile at different angles for a fixed radial positions, r^*, we could have induced from the analysis of the cof^*h profile and values that the first liquid front would be located between the first local maximum and local minimum and the second liquid front between the second local maximum and second local minimum. This means that we could state that $\zeta_A \in (25.7°, 51.4°)$ and that $\zeta_B \in (141.6°, 167.1°)$, i.e. that $\zeta_A = 38.6° \pm 12.8°$ and $\zeta_B = 154.3° \pm 12.8°$. These results would be the same independently of the radial position, r^*, chosen for placing the temperature gauges. With these results, the error in liquid front positions is given by the angular distance between nodes, or between what could be temperature gauges, i.e., 12.8°. In principle, these results suggest that having a higher number of nodes/sensors (more detailed temperature profile) the error might be reduced. Nevertheless the error is not always equivalent to the distance between temperature nodes but is limited to a minimum value depending on the thermal conductivity of the solid: the lower it is, the higher the accuracy. On the other hand, an adequate interpolation—by cubic splines, for example—of a non-detailed profile could reduce the error to a value close to the minimum value [12]. These statements are based on the results obtained from other ANSYS simulations, in which a higher number of nodes and different thermal conductivities (between 37 and 7 W/m K) have been used.

4. Validation with experimental results

Two pipe samples with the same geometry as the one described in the simulation validation have been used, i.e., carbon steel pipes with an inner/outer diameter of 50/70 mm and a length of 10 cm. The samples were partially immersed hi water inside an autoclave (Fig. 6). This autoclave is a closed thermal and mass system that allows control of operation temperature during experiments. The external heat flux is applied by a resistance wire coiled externally to every sample (Fig. 7). Six K-type thermocouples (T1–T6 in Fig. 7), at different angular positions, give the experimental temperature profile to be used afterwards. The angular distance between all these thermocouples is 36° except between T1 and T2, where it is 18°. Another thermocouple (T7) serves to check the symmetry of the temperature profile. The measuring ends of the thermocouples are placed at 3 mm from the inner surface of the pipe, i.e., at

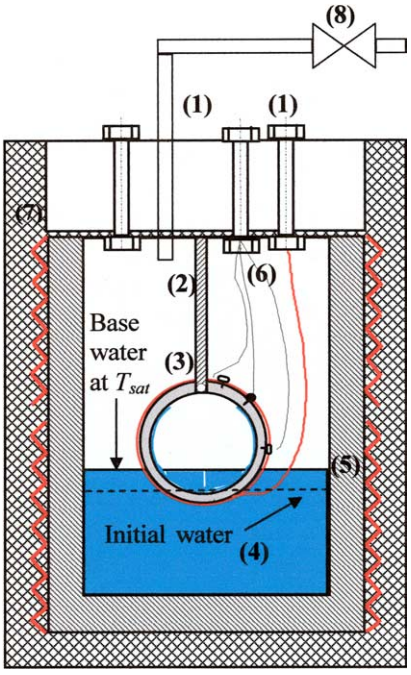

Fig. 6. Schematic description of measuring set up. (1)—feedthroughs, (2)—sample positioning bar, (3)—pipe sample, (4)—liquid level, (5)—pressurised chamber, (6)—thermocouples and second power supply wires, (7)—chamber supply heaters, (8)—security tared valve.

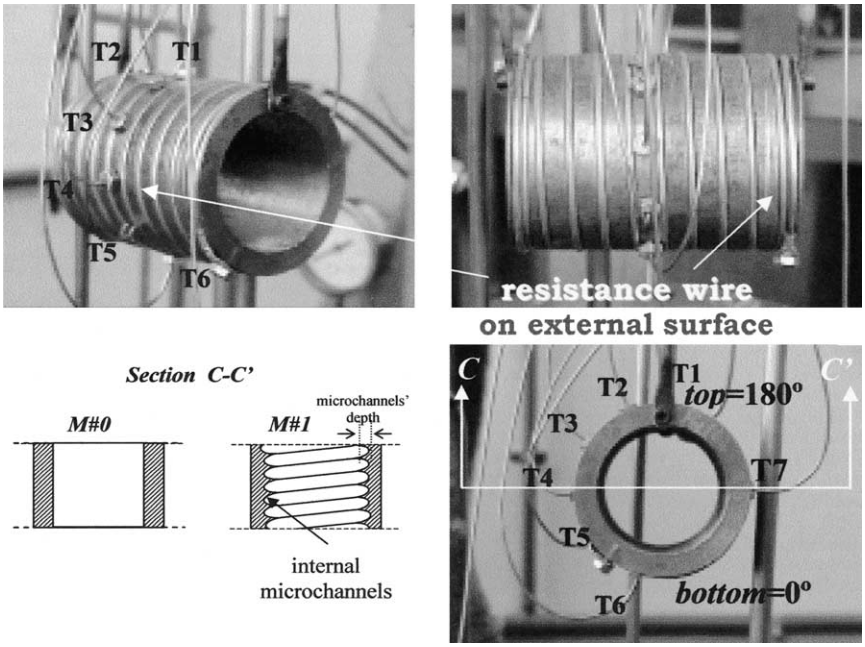

Fig. 7. Photographs of a sample ($M\#1$) already instrumented, before introducing it into the autoclave.

$r^* = 28 \times 10^{-3}$ m. Experiments at different saturation temperatures, from 100 °C up to 266 °C, and different external power supplies, from 34 W up to 1202 W, were carried out. The amount of mass water is the minimum necessary to cover the bottom of the inner surface of the sample at ambient temperature, which is why the portion of the sample that is immersed in every experiment is determined by the operating temperature (T_{sat}), which causes thermal expansion of the water.

4.1. Sample M#0

This is a normal, smooth pipe. This implies that, for a given saturation temperature and independently of the external power applied, inner (ζ_B) and outer (ζ_A) liquid front angular positions are exclusively determined by the level up to which the sample is immersed (Fig. 8). Only when the sample is half immersed $\zeta_A = \zeta_B = 90°$, but in all other possible situations there is always an angular difference between ζ_A and ζ_B of up to 45° (Fig. 9). Taking this last datum into account, as well as the fact that the angular separation between thermocouples is 36°, we can predict from the beginning that with only six thermocouples covering 180° we will not be able to distinguish between ζ_A and ζ_B.

In Table 1 the experimental conditions and results obtained by the analysis of the parameter cof^*h are shown. A short example may serve to clarify the method for obtaining such results. For an operational or satura-

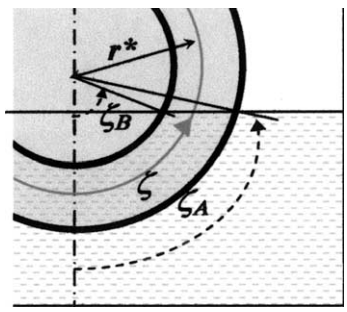

Fig. 8. Detailed figure of liquid front positions in sample $M\#0$.

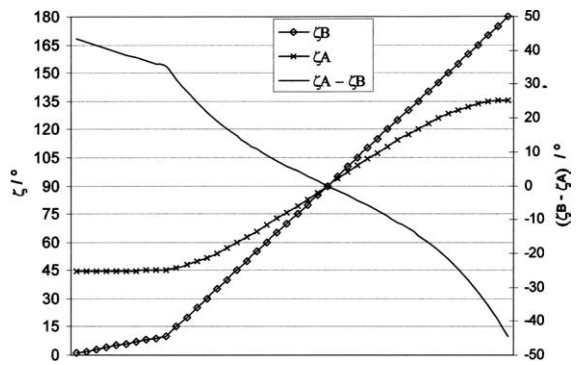

Fig. 9. Correlations in sample $M\#0$ between external, ζ_A, and internal, ζ_B, liquid front angular positions depending on how much the sample is immersed.

Table 1
Results from the analysis of cof^*h from experimental temperature profiles for samples $M\#0$ and $M\#1$

Sample	Operation temperature, T_{sat} (°C)	External power supply (W)	Liquid front position at outer surface, ζ_A (°)	Liquid front position at inner surface, ζ_B (°)
$M\#0$	100	34 ± 3		40°–80°
		67 ± 4		
		111 ± 5		
		137 ± 5(2)		
	150	191 ± 6(2)		40°–78°
		260 ± 7(2)		
	186	748 ± 12(2)		60°–110°
	200	252 ± 7		67°–90°
		417 ± 9		
		515 ± 10(2)		
		623 ± 11(2)		
		742 ± 12(2)		
		870 ± 13		
	220	860 ± 112(2)		76°–110°
	225	411 ± 9		60°–110°
		614 ± 11		
	250	721 ± 12(2)		60°–100°
		846 ± 13(2)		
		981 ± 14(2)		
		1126 ± 15(2)		
		1202 ± 16		
$M\#1$	100	137 ± 5	20°–55°	80°–126°
	125	264 ± 8	18°–53°	90°–125°
	150	260 ± 7	53°–125°	160°–180°
		642 ± 12		150°–180°
	266	1186 ± 15	60°–162°	180°

tion temperature of 100 °C several experiments have been carried out applying different external power supplies (see Table 1). The experimental thermal maps obtained for the power supplies of 67 ± 4 and 111 ± 5 W are shown in Fig. 10. As expected the temperatures are higher for the highest external power supply. A cubic spline interpolation has been used to get more-detailed temperature profiles. Having the analytical expression for this adjustments, the calculation of the term $\nabla^2 T_j^*$ is straightforward. The values of cof^*h obtained are presented in Fig. 11. In such profiles only one slope change appears, located, as expected, in a similar angular range. It is this range which defines where the inner and outer liquid front positions are located. Up to an angle of 40° the cof^*h values are approximately 10^3 W/m^{2}K, which are of the order of heat transfer coefficients

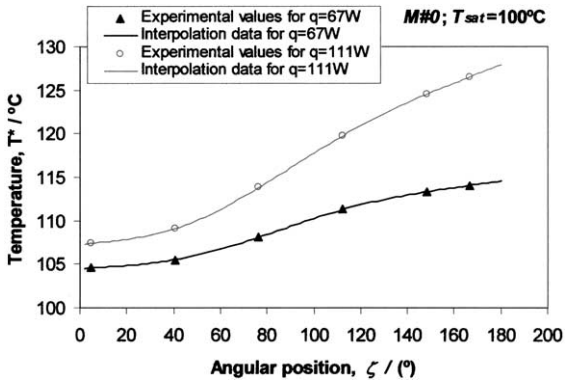

Fig. 10. Temperature profiles at $r^* = 28 \times 10^{-3}$ m for sample $M\#0$ at $T_{sat} = 100$ °C.

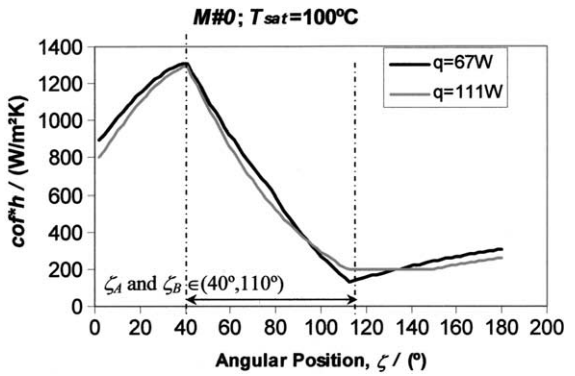

Fig. 11. Values of cof^*h obtained from Eq. (5) and using the thermal profiles presented in Fig. 10.

between solid and liquid phase. At angles of approximately 110° and above, the cof^*h values are always lower than 400 W/m^{2}K, which reflects that, from this point onwards, the solid transfers energy to a gas phase. The range reduction from (40°, 110°) to (40°, 80°)-value range shown in Table 1- is due to the intersection between the angular ranges for ζ_A and ζ_B obtained with other experiments at $T_{sat} = 100$ °C under other different external power supplies.

The experimental angles for ζ_A and ζ_B for $M\#0$ shown in Table 1 have been verified with a direct calculation of such angles from the mass of water employed to partially fill the autoclave, and taking into account the variation of water specific volume with temperature and the experimental errors [12].

4.2. Sample $M\#1$

Externally sample $M\#1$ is a smooth pipe but in its inner surface vertical microchannels of 0.77 mm depth have been grooved (Fig. 7). The capillary forces promoted by these microchannels keep the inner wet front higher than the one corresponding to the smooth sample, i.e., $\zeta_B(M\#0) \leqslant \zeta_B(M\#1)$. While the outer angular positions ζ_A depend on saturation temperature only, the inner angular positions of the liquid front, ζ_B, must be considered a function not only of the capillary forces but also of the additional power supply, because the vaporisation of the liquid flowing in the microchannels limits its actuation as energy drainage.

In Table 1 the experimental operating conditions and the results from the cof^*h analysis for this sample are presented. Two different angular ranges are clearly identified for every experimental condition, distinguishing between the liquid front positions ζ_A and ζ_B. For an saturation temperature of 266 °C and a power supply of 1118 ± 15 W the ζ_B position is fixed at 180°, without any uncertainty. It is because the cof^*h values obtained

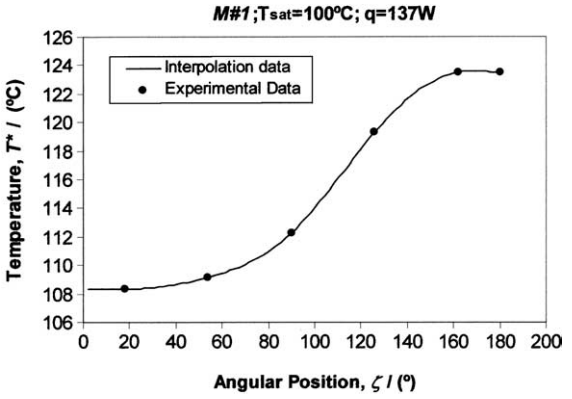

Fig. 12. Temperatures profiles at $r^* = 28 \times 10^{-3}$ m for sample $M\#1$ at $T_{sat} = 100$ °C.

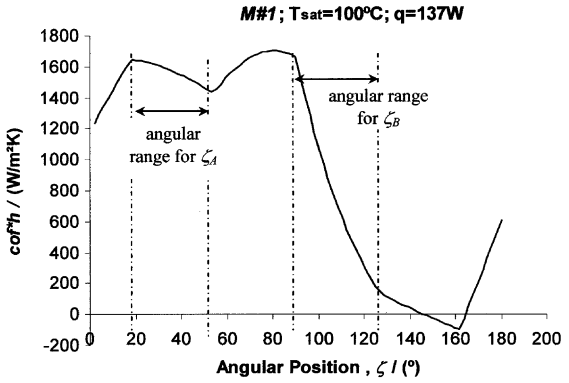

Fig. 13. Values of cof^*h obtained from Eq. (5) and using the thermal profiles presented in Fig. 12.

for this angular position leaves no doubt that the heat transfer is between solid and vapor. As an example the experimental temperature data for $T_{sat} = 100$ °C and power supply of 137 ± 5 W are shown in Fig. 12. The cof^*h profile obtained using cubic spline interpolation and Eq. (5) is shown in Fig. 13. Two slope changes can be distinguished: one that determines the outer liquid front position, or ζ_A, located in the range (20°, 55°), and the other that gives the inner liquid front position, or ζ_B, located in the range (80°, 126°). The uncertainty in both ranges is similar to the angular separation between thermocouples (36°).

5. Conclusions

The experimental methodology described in this paper can be applied to determine the liquid front positions on the surfaces of a heated 2-D solid working under two-phase flow conditions, being especially useful when visual inspection is difficult or not possible.

From a unidimensional temperature experimental data profile, an effective heat transfer coefficient here defined, cof^*h, can be calculated. The high differences between solid–liquid and solid–gas heat transfer coefficients are easily visualized through a graphic of the cof^*h parameter versus position. The liquid front positions are located thanks to the values and profile (range between consecutive local maximum and minimum) of this parameter. One advantage of this method in relation with others that appear in the literature is that the thermal behaviour of a 2D-solid can be studied with a unidimensional model that significantly reduces the mathematical complexity of the heat transfer treatment.

The local maximum and minimum positions that determine the range within which the liquid fronts are located do not depend on the distance from the two external surfaces at which the sensors are placed within the solid. This feature lends the proposed methodology a

high flexibility with regard to the positioning of the sensors, which can be adapted to the solid in question and to experimental system restrictions.

The accuracy of this method depends, although not critically, on the geometrical performance (i.e. whether the solid in question is plane or cylindrical) and on the distance between sensors. The main restriction for obtaining higher accuracy is the thermal conductivity of the solid: the lower it is, the lower the error obtained in the liquid front positions. The thermal conductivity of the solid determines a minimum error value, that can nearly be achieved with a temperature profile obtained by an adequate interpolation of non-detailed experimental temperature data (the adequate interpolation proposed here is cubic splines). On the other hand, the experimental errors in the data acquisition lead to a grade of uncertainty in about the same range of error associated to the proposed method. This is especially true when the method is applied in the designing of capillary systems to work under predetermined requirements: the errors in the experimental determination of their characteristic parameters are much higher than the uncertainty due to the method itself.

The methodology has been validated with ANSYS simulations, and applied to find out the inner and outer liquid front positions in carbon steel pipes with inner/outer diameters of 50/70 mm and a length of 10 cm, with and without capillary system in the inner face. Experiments were carried out by partially immersing the samples in water and working under saturation temperatures ranging from 100 to 266 °C with external power supplies from 34 to 1200 W.

References

[1] S. Yoshida, T. Matsunaga, H.P. Hong, K. Nishikawa, Heat transfer to refrigerants in horizontal evaporator-tubes with internal, spiral grooves, in: P.J. Marto (Ed.), Proc. 1987 ASME-SSME Thermal Eng. Joint Conf., vol. 5, 1987, pp. 165–172.

[2] J. Weisman, J. Lan, P. Disimile, Two-phase (air–water) flow patterns and pressure drop in the presence of helical wire ribs, Int. J. Multiphase Flow 20 (5) (1994) 885–899.

[3] P. Geskes, Flow patterns in annular geometry of an absorber pipe with DSG by water injection, in: J.C. Chen, F. Yasunobu, R. Nelson (Eds.), Convective Flow Boiling: Proc. Convective Flow Boiling, Taylor & Francis, 1996, pp. 371–376.

[4] T. Shedd, Ty.A. Newell, Visuaization of two-phase flow trough microgrooved tubes for understanding enhanced heat transfer, Int. J. Heat Mass Transfer 46 (2003) 4169–4177.

[5] M. Eck, P. Geskes, O. Goebel, U. Hermann, F. Lippke, E. Rojas, W.D. Steinmann, Final Task Report on DSG Applied Research (Doc. ID. DISS-MQ-QA-32. Confidential) of the Direct Solar Steam (DISS)—phase I project. JOR3-CT95-0058.

[6] X.F. Peng, G.P. Peterson, Capillary-induced rewetting in a flat porous cover layer, Int. J. Heat Mass Transfer 35 (2) (1992) 319–327.

[7] X.F. Peng, G.P. Peterson, X.J. Lu, Analysis rewetting in circular channels with internal grooves, J. Thermophys. Heat Transfer 7 (2) (1993) 334–339.

[8] S.P. Malyshenko, A.V. Zuev, A.B. Andrianov, Heat transfer intensification and thermal stability enhancement for direct steam generation solar receivers using porous coatings, Proc. 7th Int. Symp. Solar Concentr. Technol. 4 (1994) 934–942.

[9] M. Fishenden, O.A. Saunders, An Introduction to Heat Transfer, Oxford University Press, London, 1950.

[10] W.M. Rohsenow, A method of correlating heat-transfer data for surface boiling of liquids, ASME J. Heat Transfer 74 (1952) 969–976.

[11] L.A. Bromley, Heat transfer in stable film boiling, Chem. Eng. Prog. 46 (5) (1950) 221–227.

[12] M.E. Rojas, Mejora de la transferencia de calor en flujo horizontal bifásico, Aplicación a colectores solares cilindro-parabólicos, PhD thesis, Universidad Complutense, Madrid, Spain, 2003.